Bacterial Cellulose Films: Influence of bacterial strain and drying route on film properties

Muling Zeng, Anna. Laromaine*, Anna Roig

Institut Ciència de Materials de Barcelona, Campus UAB, 08193 Bellaterra, Spain.

E-mail: alaromaine@icmab.es

Abstract

Bacterial cellulose is increasingly used as reinforcing material or scaffolds for smart electronics or biomedical applications due to its multifaceted advantages like natural abundance, eco-friendliness, cost-effectiveness, biocompatibility and easy chemical modification. Structural and functional properties of bacterial cellulose depend on the microstructure of the material, which in turn is influenced by the cellulose´s origin. This paper reports the production of bacterial cellulose thin films from two bacterial strains, *Gluconacetobacter Xylinus* and *Gluconacetobacter Europaeus*, and three methods of drying the thin films; at room temperature, freeze drying and supercritical drying. We have undertaken for the first time a comparative study of how several material's properties such as porosity, transparency, water absorption capacity and mechanical properties are or not affected, and thus can be tuned to some extent, by selecting the bacterial strain or the drying method. For instance, using supercritical drying, we obtained mechanically robust and extremely light films with up to 96 % of porosity, and with a water absorption capacity up 110 times their dried weight. Finally, we suggest the appropriate choice of strains and drying methods for different applications, for instance to obtain cellulose composites with high efficiency in the loading of the components.

Introduction

The interest in cellulose and cellulose composites materials have recently expand due to their sustainable and environmentally friendly sources (vegetable or bacterial), their functional and structural properties and applications.(Hu et al. 2014) Its facile derivatization and formulations yields organic-inorganic cellulose composites materials which usually as films find application in oil and water absorbents,(Sai et al. 2013; Nata et al. 2011; Ul-Islam et al. 2012b; Jin et al. 2011) organic light emitting diodes, (Ummartyotin et al. 2012) flexible and transparent electronics(Wicklein and Salazar-Alvarez 2013) to name a few.(Klemm et al. 2011)

Vegetal cellulose is extracted from plants and wood and bacterial cellulose (BC) is produced by microbial fermentation. Although with higher production cost than vegetal cellulose, BC offers a pure biopolymer that exhibits a higher degree of polymerization and better crystallinity than plant's cellulose.(Ross et al. 1991) They exhibit high water content, high elasticity and mechanical stability. Importantly, BC does not contain lignin, hemicelluloses and pectin, non-degradable molecules, associated to the toxicity of celluloses.(Ul-Islam et al. 2012a; Czaja et al. 2007) Therefore, BC composites not only find application in electronics or optics but also in the food industry(Shi et al. 2014) (calorie-free dessert)(Kalia et al. 2011) and in medical fields (tissue engineering,(Svensson et al. 2005; Andrade et al. 2013; Saska et al. 2012) and wound healing patches(Ul-Islam et al. 2012a; Fu et al. 2013)).

The blending of components to form cellulose composites although it is simple, offers a poor control of the mixture´s homogeneity decreasing the performance of cellulose composites. In order to fabricate homogeneous cellulose composites with high loading of components, researchers take advantage of the high adsorption capability and structural properties of the cellulose fibers. The cellulose origin and processing treatment strongly influence the final characteristics of the composites.(Pinto et al. 2012)

51   In order to improve the BC films adsorption capabilities and porosity, we dried the harvested

52   BC thin films using three different methods, room temperature (RD), freeze drying (FD) and

53   using CO_2 supercritical (SCD) without any further mechanical treatments to the cellulose

54   fibers. We obtained a plethora of materials with different adsorption capabilities and

55   improved structural properties with few fabrication steps. The selected physical processes

56   evaporate the solvent content within the film, while minimizing hornification processes of the

57   cellulose fibers. When drying at room temperature (RD), capillary pressures of the water

58   meniscus exert a compressive force in the pores of the films that may induce the modification

59   of the structure, density and porosity of BC films. Freeze drying (FD) process dries the film

60   through sublimation of solid water after the BC films have been plunge-frozen in liquid

61   nitrogen. Supercritical drying (SCD) involves the exchange of the water solvent within the

62   BC film by ethanol, a final exchange with liquid CO_2 in the reactor and the final evacuation of

63   the CO_2 in supercritical phase. Evacuation of solvents in supercritical conditions is commonly

64   used to produce aerogels which is a term given to open pore materials presenting low density

65   and large specific surface area. The most known aerogels are silica,(Murillo-Cremaes et al.

66   2010; Moner-Girona et al. 2003; Martin et al. 2008; Budunoglu et al. 2011) carbon,(Wu et al.

67   2013; Mecklenburg et al. 2012) organic-inorganic aerogels(Hendel et al. 2013; Ennajih et al.

68   2012) and more recently thick pieces of BC aerogels have also been reported (Hendel et al.

69   2013; Liebner et al. 2010; Cai et al. 2008; Russler et al. 2012).

70   Additionally, we compared the drying methods along with the BC films produced from two

71   bacterial strains, *Gluconacetobacter Xylinus* (GX) and *Gluconacetobacter Europaeus* (GE), to

72   evaluate the impact of the bacterial origin. *Gluconacetobacter Xylinus* is the most extended

73   bacteria used to produce cellulose, some reports justifies its commercial interest due to the

74   fast cellulose production speed. *Gluconacetobacter Europaeus* (formerly *Acetobacter*

75   *Europaeus*) is one of the most prominent acid acetobacter bacteria species isolated from

76   industrial submerged vinegar fermenters with high resistance to acetic acid and it is much less

77   studied for cellulose production that the GX counterpart.(Andrés Barrao et al. 2011)

78   We compared the microstructure, water holding capacity, transparency and mechanical

79   properties of BC films of less than 100 µm in thickness, and produced by two bacterial strains.

80

81   **Experimental Section**

82   Bacterial strains *Gluconacetobacter Xylinum* (GX) (ATCC 11142)(Yamada et al. 1997) and

83   *Gluconacetobacter Europeaus* (GE) (MF03)(Yamada et al. 1997) were purchased from CECT

84   (Spain).

85   Glucose, peptone, yeast extract and agar were purchased from Conda Lab, and the NaOH,

86    $Na_2HPO_4 \cdot 12H_2O$ and citric acid monohydrate were bought from Sigma Aldrich and used as

87   received.

88

89   **Synthesis of BC**

90   GX and GE were grown on a solid agar and a single colony was expanded in liquid media for

91   3 days. Then, 8 ml solution was transferred to an Erlenmeyer of 1L with 200 mL of liquid

92   media. A thin film of bacterial cellulose grew on top of the liquid media over 5 days for GX

93   and 10 days for GE. Culture media for GX consisted of 20 g/L glucose, 5 g/L peptone, 5 g/L

94   yeast extract, 1.15 g/L citric acid monohydrate and 6.8 g/L $Na_2HPO_4 \cdot 12H_2O$. Culture media

95   for GE was composed of glucose 50 g/L and yeast extract 10 g/L.(Liebner et al. 2010; Kim et

96   al. 2010; S. Hestrin 1954)

97   BC films harvested from the air/liquid interface were immersed in ethanol. Subsequently they

98   were transferred to deionized (DI) water and boiled for 40 min, four times more with 0.1 M

99   NaOH at 90 °C for 20 min and finally, neutralized with DI water for 24 h.

100

101

Drying methodologies

Never dried Bacterial cellulose (BC) films were cut into a rectangular shapes of 1 x 2 cm.

Before drying, samples were placed over a sheet of chromatography paper and kept between

two glass slides during the drying process. We created an accordion-like setup for each drying

methodology, up to 10 BC films were placed in the same setup. BC fibers were not

mechanically modified and the BC film maintains the shape from the bacterial culture. Figure

S1 presents schematics and pictures of the drying setup.

Room temperature drying method (RD)

BC films placed in the accordion setup were kept at room temperature for 4 days until the BC

films were completely dried.

Freeze-drying method (FD)

We plunge-froze the samples in the accordion setup with liquid nitrogen for 5 min in a 50

mL falcon tube. After, they were placed in the freeze-drier for 12 h. Freeze-drying of the

samples was performed with a LYOQUEST-85 freeze drier (Telstar) at -80 º C, below 0.005

mbar for 12 h.

Supercritical CO$_2$ drying method (SCD)

BC films were subjected to a solvent exchange step, which was performed by gently shaking

them in absolute ethanol. After 6 and 12 h, the gels were transferred two times to a fresh

ethanol bath without shaking. After another 6 h in ethanol, the resulting alcogels were dried.

Supercritical process was performed on SCF 300 ml Plant in MATGAS, Spain. Alcogels BC

films were placed in the accordion setup and loaded into a 300 ml autoclave vessel filled with

ethanol. The autoclave was pressurized to 100 bar at room temperature. We exchanged the

ethanol with liquid CO$_2$ flowing at 1 kg/h for 1.5 h. We heated the reactor at 45 $^{\circ}$C; with a

CO$_2$ flow of 1 kg/h for 1 h (these are the SCD conditions, 45 $^{\circ}$C, 100 bar). After the drying

period, we slowly depressurized the autoclave and removed the dry aerogels.

128

Characterization of BC films

Fourier Transform Infra-Red Spectroscopy with Attenuated Total Reflectance (FTIR-ATR)

We folded 5 times the BC films and placed them onto the Universal diamond ATR top-plate (Perkin Elmer). IR spectra were acquired using a PerkinElmer FT-IR Spectrum One with U-ATR at 4 cm^{-1} resolution, between 4000 to 500 cm^{-1} using 4 scans and a pressure force between 80 % and 90 %.

X-Ray Diffraction (XRD)

XRD patterns of the BC films were recorded using an X-Ray Diffractometer (Siemens, Model D-5000), using a Cu anode with $\lambda_{K\alpha1}$=1.540560 Å and $\lambda_{K\alpha2}$ =1.544390 Å in the 2θ range of 3 – 60° using a step of 0.02 °/min. All samples were fixed flat on a silicon wafer to perform the measurement.

We calculated the crystallinity of BC films using the height of peaks (CrI)(Segal et al. 1959; Wang et al. 2008) computed them using Spectrum Viewer Basic 2.6. The height of the peak at (200) represents the crystalline part $I_{(200)}$ and the minimum height between (200) and (110) peaks the amorphous part, $I_{(am)}$. We also used the same equation 1 but instead of the height of the peaks, we used the area, and we obtained the same results. (Table S1)

Equation 1 $$CrI = (I_{(200)} - I_{(am)})/ I_{(200)}$$

The crystal size using the (200) peak was computed using Scherrer´s equation:(Mansikkamaki et al. 2007; Zhang et al. 2001)

Equation 2 $$L (h\,k\,l) = k\,\lambda / (B\,cos\Theta)$$

Where L is the crystallite domain, λ is the X-ray wavelength, Θ is diffraction angle in radians and B is the full width at half maximum of peak ($B^2 = B_{total}^2 - B_{instrument}^2$), B_{total} is the integral breadth in radians of diffraction angle and $B_{instrument}$ is the instrumental integral breadth in radians and k (Scherrer's constant) is a dimensionless shape factor. The shape factor has a

154 typical value of about 0.9, but varies with the actual shape of the crystal, k = 0.94 was chosen

155 in our case. (Das et al. 2010; Dietrich et al. 1987)

156

157 **Scanning Electron Microscopy (SEM)**

158 All BC film samples were gold coated for 1 min at 20 mA, approximately with 1 nm of gold

159 with a K550 Sputter Coater (Coating Attachment Emitech. Ashford, UK). Samples were

160 placed on a SEM aluminum substrate over a carbon tape adhesive. Images of Scanning

161 Electron Microscopy (QUANTA FEI 200 FEG-ESEM) were taken at high vacuum

162 conditions, an acceleration voltage of 10-30 kV, an electron beam spot of 2.5, a pressure of 2

163 to 8×10^{-4} Pa and a distance of 2 – 6 mm. SEM images of BCE-RD samples were acquired at

164 the low vacuum conditions, an acceleration voltage of 10 kV, an electron beam spot of 2.5, a

165 pressure of 40 Pa and a distance of 5 mm to improve the image acquisition.

166

167 Thickness of the films were computed using an optical microscope in differential interference

168 contrast mode (n=10) (Olympus IX-71, program of Stream Essential 1.7).

169

170 **Thermal Gravimetric Analysis (TGA)**

171 Thermal gravimetric analysis of the BC films was performed with a TGA-DSC/DTA analyzer

172 (NETZSCH STA 449 F1 Jupiter, ICMAB) with a heating rate 20 °C/min from room

173 temperature to 800 °C in air.

174

175 **Water Absorption Capacity (WAC)**

176 BC films grown for 10 days were dried and weighted. We immersed them in DI water for 1 h,

177 2 h and 2 days. Excess water was removed at each time and measured the weight again. The

178 water absorption capacity was defined by:

179 Equation 3 $\qquad\qquad W = (W_{wet} - W_o) / W_o$

180   W_{wet} (weight of wet BC films), W_o (initial weight of the dried BC films).

181

182   **Optical transmittance**

183   The optical transmittance of the films was measured using an ultraviolet-visible (Uv-vis)

184   spectroscopy (Shimadzu UV/VIS UV-2102 spectrometer) in the 250 nm to 800 nm range.

185   Samples were carefully cut into the rectangle shapes as one side of the cuvette; they were

186   placed in the front side of the Uv-vis spectroscopy cuvette in order to take the spectrum.

187

188   **Mechanical properties**

189   Penetration depth at maximum load (0.4mN), Hardness, Young's modulus and Elastic

190   parameter (EP%) of BC films were obtained with a nanoindenter (Nanoindenter XP system)

191   with a Berkovich diamond indentation tip. All samples were cut into 0.5 x 1 cm and were

192   fixed flat on the holder using double-sided tape, without any further preparation. Indentation

193   curves were obtained at a loading and unloading rate of 0.08 mN/s and maximum load of 0.4

194   mN. BC films were measured 5-10 times in regions separated within 5 μm each measurement

195   in order to evaluate and average the whole surface. Two different BC films samples were

196   evaluated for each type of material.

197   EP parameter was computed with:

198   Equation 4: EP %= (penetration depth at max loading - penetration depth after unloading)/

199   (penetration at max loading) %.

200   **Evaluation of mechanical properties and directionality of fibers**

201   BC-SCD films (1 × 2 cm) were cut into 2 smaller pieces (1 × 1 cm). One was fixed flat on the

202   holder by double-sided tape; another piece was turned 90 ° and then fixed on the same holder.

203   Pieces were tested with the same setup conditions by Nanoindenter XP system.

204
205
206

Results and discussion

Production of thin BC films

Two bacterial gram-negative strains, *Gluconacetobacter Xylinum* (GX) and

Gluconacetobacter Europeaus (GE) produced thin films of bacterial cellulose (BC). First,

harvesting times of the two strains were adjusted to obtain similar film thicknesses. 10 days of

culture for GE and 5 days for GX yielded BCE and BCX films of comparable thicknesses at

the top of the culture liquid media of an erlenmeyer at 25°C, Figure 1A. Prior to films drying,

BC layers were cleaned to remove any bacterial detritus following a previously reported alkali

procedure.(Liebner et al. 2010; George et al. 2008) After the alkali treatment, BC films

increased their transparency, Figure 1B.
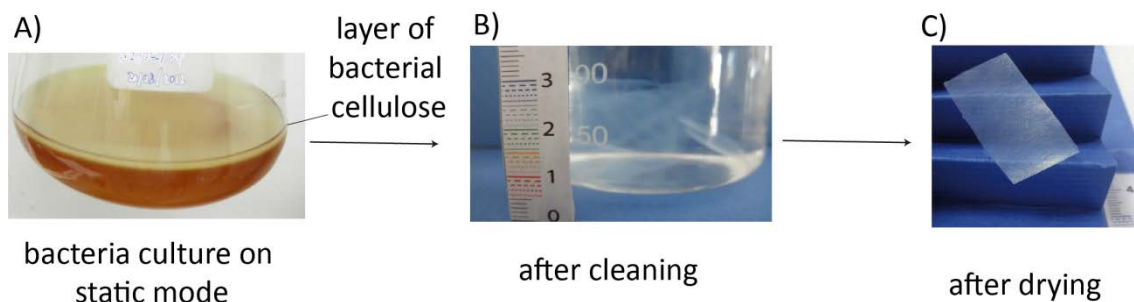
Figure 1. **(A) Picture of a BC layer on top of the bacteria culture liquid media. (B)**

Cleaned BC films obtained after the NaOH treatment. (C) Picture show a final BC film

dried and the accordion setup were BC films are held during the drying process.

Films were then dried using three methods: a) solvent evaporation at room temperature (RD),

b) freeze drying (FD) and c) using supercritical CO_2 (SCD). In all cases, wet films were

placed in a home-made holder. A paper accordion construct held BC films in between two

glass slides to ensure regular shapes and prevent bending during drying, Figure S1. This

design afforded flat and thin films of less than 100 µm in thickness, Figure 1C, with few steps

and different properties.

Characterization

BC films are a semi crystalline material and produce broad diffraction peaks. Figure 2A

shows the XRD patterns of BCE films treated with different drying methods. Native cellulose

is present in two different crystalline cellulose I modifications (I_α and I_β), which can be found

alongside each other at $2\Theta = 14.24$ and 17.36 corresponding to <1-10>, <110> respectively,

the I_α / I_β ratio depends on the origin and the processing of the cellulose. (Klemm et al. 2005;

Atalla and Vanderhart 1984) After the alkali treatment, all BC films showed two main peaks

at $2\Theta = 14.6$ and 22.6 arising from crystalline planes <1-10> and <200>, respectively, and

BCE-SCD also showed a small peak at ~17.1° (2Θ) arising from the <110> plane.

Relative crystallinity (CrI) of BCE-SCD, BCE-FD and BCE-RD films was calculated using

the intensity of the <200> peak considering equation 1 and yielding 82.9 %, 75.6 % and

72.5 %, respectively. In addition to the highest crystallinity observed for the BCE-SCD films,

those also present a slightly smaller crystalline domain (15 nm) as compared to FD (16 nm)

and RD (17 nm). Since all BC films derive from the same initial sample, any variations in the

crystallinity and crystal size are caused by the drying methods. The higher temperature of the

drying with SCD, 45ºC, could afford this small increase of cristallinity. We obtained the same

patterns for BCX films, indicating that the cristallinity of the cellulose fibers are independent

of the bacterial strain.

The IR spectrum of the BC films are characterized by a strong and broad band around ν (CH)

(OH):3342, 3347 cm^{-1} corresponding to the overlap of the stretching vibrations of C-H and O-

H respectively and a strong peak at ν (CH_2 and CH) around 2895 cm^{-1}. Cleanliness of the

materials can be monitored by the decrease of the amide I (ν (strong)$_{C=O}$: 1642 cm^{-1}) peak,

Figure 2B.(Klemm et al. 2001)
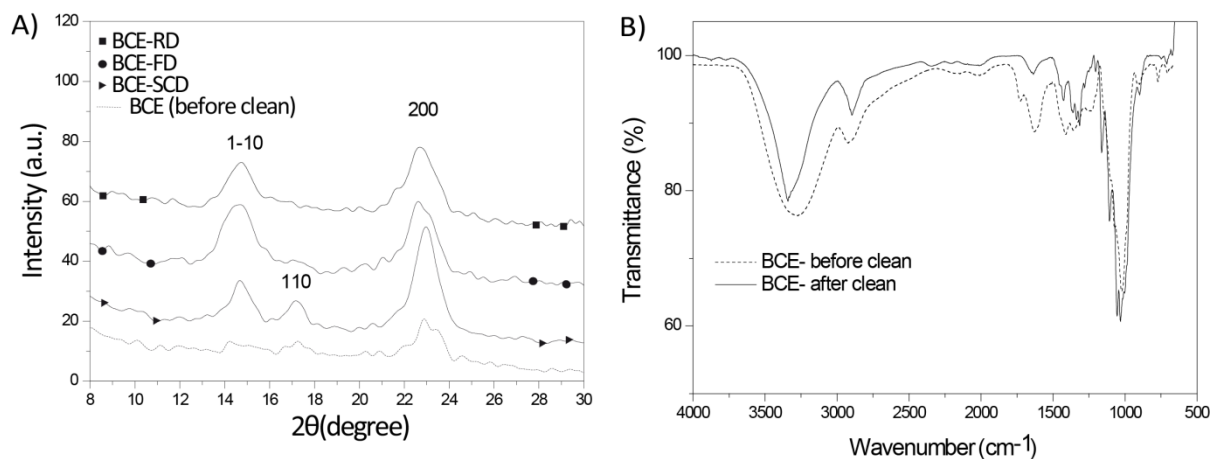
Figure 2. (A) X-ray diffraction pattern for BCE- RD, BCE- FD, BCE- SCD and non cleaned BCE film. (B) FTIR spectra for a non-cleaned BCE film and a BCE film after cleaning.

Thermogravimetric analysis of BC films showed the typical single step thermal degradation profile with a decomposition temperature around 350 °C, Figure S2. The residual mass of BC films is less than 4 % indicating BC films were free of impurities. These values agree to previously TGA analysis reported for BC materials after alkali treatment. (George and Ramana 2005)

The thickness and size of wet and dry films were measured using an optical microscope in differential interference contrast microscopy mode. Table 1 summarizes the film thicknesses of the dried films (n=10). For both strains, films dried in SCD conditions are thicker than films obtained by FD and RD. The elimination of the solvent meniscus during supercritical solvent evacuation, avoids the effects of the capillary forces, as described previously for other aerogel materials. The initial thickness of the wet BC films were around 200 µm and after drying the computed thickness of all BC films decreased, ranging from 67 µm to 24 µm.

Density values (ρ) were determined from weighting the materials and measuring the BC films' volume. Films produced by GE are extremely light materials with densities around 0.08 - 0.05

11

273   g/cm^3 showing only a slight dependency of the density with the drying method but strong

274   influence of the bacterial source. Densities of the BCX films are in the 0.16 - 0.6 g/cm^3 range

275   and they strongly depend on the drying method used. BCX films dried by SCD are lighter

276   than FD and RD ($\rho_{BCX-RD} > \rho_{BCX-FD} > \rho_{BCX-SCD}$), although they are still two times denser than

277   any BCE film ($\rho_{BCX} > \rho_{BCE}$), see **Table** 1.

278   From the density values one can evaluate the total porosity of the films from the equation:

279   Total porosity (ϕ) = 1- ($\rho_{BC\ film}/ \rho_{cellulose}$); where we have assumed a $\rho_{cellulose} = 1.5$ g/cm^3

280   (Mwaikambo and Ansell 2001; Sehaqui et al. 2011; Sun 2005) for both strains. Following the same trend as for the

281   density, we observed that BCE films have a porosity larger than 94 % for the three drying

282   methods. On the other hand, BCX films are less porous and their porosity strongly depends on

283   the drying method used. We believe that the slow formation of the cellulose fibrils in GE

284   influences the microstructure of the film, forming fibrils more resistant to compact and finally

285   affording a more spongy structure.(Mwaikambo and Ansell 2001; Sehaqui et al. 2011; Sun

286   2005).The porosity, density are strongly affected by the bacterial strain and the drying
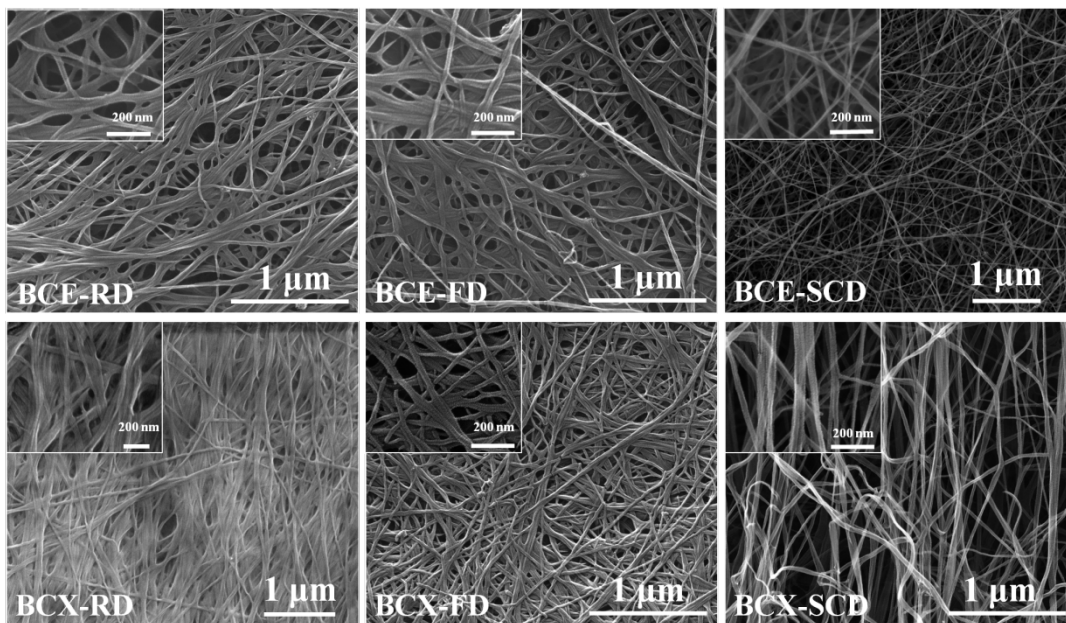
287   methods.

288

289   **Microstructure of the BC film**

290   BC films present an open porous network of cellulose fibers confirmed by scanning electron

291   microscopy (SEM), Figure 3. Similarly to previous reports,(Siro and Plackett 2010; Schutz et

292   al. 2012) BC films show a hierarchical structure with pores of different sizes from macro to

293   micro. For both strains, SCD drying method offer the most open structure and a higher

294   presence of individual fibrils than FD and RD films. BET measurements of the porosity of the

295   thin films provided partial results of the porosity of the thin BC films skewed towards the

296   mesoscale.

297   Individual cellulose fibrils measured by SEM are approximately 18 ± 2 nm in thickness

298   independently of the strain and the drying method used. Thus, the strain used or the drying

methods do not seem to influence the fibril size which is somehow surprising considering the difference in the cellulose growth rate of the two strains. In contrast, a detailed observation of the images showed that the drying method impact the fiber entangling. Analyzing in detail several SEM images, we computed that for both strains, 85 ± 2 % of the fibers form bundles in the films dried at RD and FD whereas we detect just a 38 ± 2 % of the fibers forming bundles in SCD films. Moreover, BCX-SCD is the material with the most differentiated microstructure since we distinguish higher number of individual fibers, less entanglement and some degree of directionality of the fibers in comparison to the rest of the films. Some detailed studies to elucidate if fiber directionality induces anisotropic mechanical behavior will be analyzed.

Figure 3. SEM images of the BC films obtained after different drying conditions. Inserts show higher magnification images of the films.

	Drying method	RD		FD		SCD	
	Strain	BCE	BCX	BCE	BCX	BCE	BCX
Structural	Film Thickness (µm)	24±2	37±2	34±2	40±4	58±3	67±2
	Density (g/mL)	0.08± 0.01	0.59± 0.03	0.06± 0.01	0.32± 0.02	0.05± 0.01	0.16± 0.01
	Total Porosity (%)	94±2	60±2	95 ±2	79±2	96±2	89±2
	Fibers diameter	17±2	19±3	20±4	19±3	16±2	20±4

		(nm)						
	WAC	1st cycle	39.5	37.3	15.8	15. 8	109.4	66.6
		after 3 cycles	15.3	14.2	92.3	50.2	19.8	19.4
		Decrease (%)	61	62	42	68	82	71
Mechanical		Penetration depth at 0.4mN load (µm)	3.9±0.4	1.1±0.1	4.1±0.4	1.4±0.3	3.2±0.5	4.3± 1.5
		Young modulus ("E")(MPa)	198±50	659±90	204±50	601±200	238±20	198±30
		Hardness ("H")(MPa)	34±20	39±9	20±8	26±10	20±5	19±20
		EP (%)	59±7	39±3	53±4	33±3	52±5	48±10

Table 1. Summary of the structural and mechanical values obtained for the BC films.

Water absorption capacity (WAC)

Cellulose materials are good absorbents, this property identifies them as excellent candidates for instance for organic pollutants, absorbents and catalysts (improve efficiency of enzyme loading).(Wu et al. 2013; Shezad et al. 2010) This property is also exploited in order to create cellulose composites with high yield of the different components, for instance in antibactericidal BC patches that need a homogeneous and high loading of Ag nanoparticles.(Ul-Islam et al. 2012a; Ul-Islam et al. 2011) We measured the water absorption capacity and evaluated how the different drying methods and therefore, the microstructure obtained influence the water absorption capacity (WAC). We dried and weighted BC films, upon immersion in distilled water at room temperature for two days they were weighted again. WAC quantifies the percentage of water absorbed in each film. We repeated two times the water absorption cycle drying them at room temperature. The weight of the dry films at the start of each WAC cycles did not change.
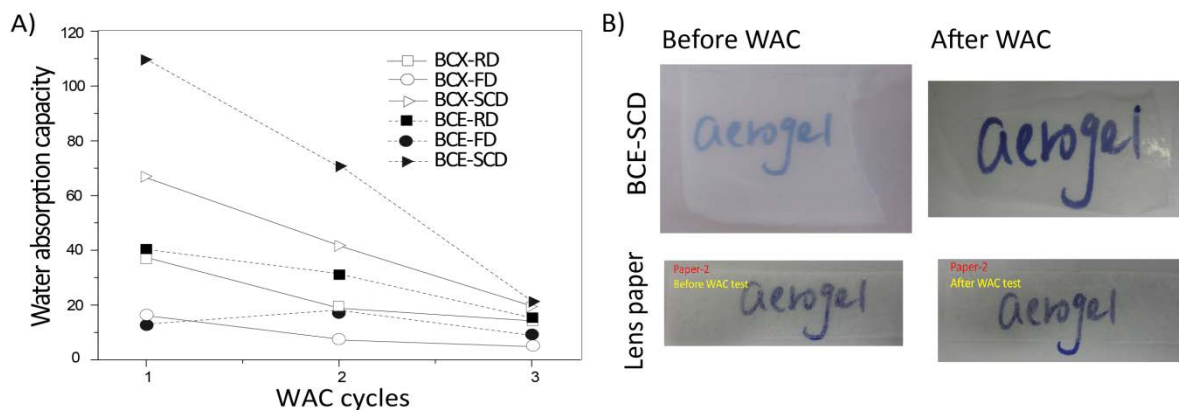
Figure 4. (A) Percentage of the water absorbed in the BC films after three wetting-drying cycles. (B) Images of the BCE-SCD films and lens paper before and after wetting.

WAC shows a strong influence of the drying method used. Supercritically dried films present the highest water absorbance capability of all the films, obtaining water absorption capacities of up to 110 times its own weight for BCE-SCD films, Figure 4A. FD films showed lower water absorption than RD for both strains. SCD drying method emerges as an ideal methodology to improve WAC in native BC films without additional mechanical processes or additives.

The ability of the films to recover the WAC capacity after drying at room temperature was evaluated performing some wetting-drying cycles. After three wetting-drying cycles, the WAC values converged for all the drying methods and the BC films still held up to 20 times their weight of water after 3 cycles, Figure 4A. We hypothesized, since in the WAC cycles we dry the films at room temperature, we compact the tridimensional structure of the film in each cycle until they all become similar. The extraordinary WAC achieved with supercritical drying methods indicates that the structure achieved could afford a methodology to create cellulose composites with high concentration of different compounds in an homogeneous fashion by absorption, such higher and more reproducible absorption of enzymes to improve their response.

15

Transparency

Evaluation of the water absorption capacity also revealed that the films increase their

transparency upon wetting. Their applications in electronics could also be expanded in water-

based applications, for instance in cell-based membranes, in skin-patches with flexible

electronics since they could help to monitor wound

healing,(http://www.ricoh.com/about/company/technology/tech/033.html) in sensors devices

where we could envisage while the liquid is transported without the need of external power,

we could image its reactivity from the change in transparency. Pictures depicting the

qualitative measurement of the transparency for lens paper, 35 µm, and the BCE-SCD film

before and after WAC cycle are shown in Figure 4B and Figure 5A. (Films are placed in

contact with the paper below). BCE-SCD film became more transparent than the lens paper

after a WAC cycle, likely related to the collapse of pores in the size range with larger visible

wavelengths scattering effect. Pictures of all the films are in Supplementary information

Figure S3. Quantification of the transparency using Uv-vis Spectroscopy was performed for

BC films. (Figure 5B for BCE and Figure S4 for BCX). BC films do not absorb above 500 nm

before and after WAC showing a higher optical transmittance compared to regular

chromatography paper of 200 µm (Paper 1) and lens paper of 35 µm (Paper 2). Initially BCE

films are more transparent than BCX films that could indicate the existence of different light

scattering effects in the films and they could reveal different surface roughness. (Yano et al.

2005) After the different WAC cycles, the optical transmittance improved for all the films.

High transparency of BC films at visible wavelengths and the biological origin of the

cellulose could appoint this material as a suitable matrix to biological applications where the

optical visualization through the material is necessary as for instance in cell culture surfaces.
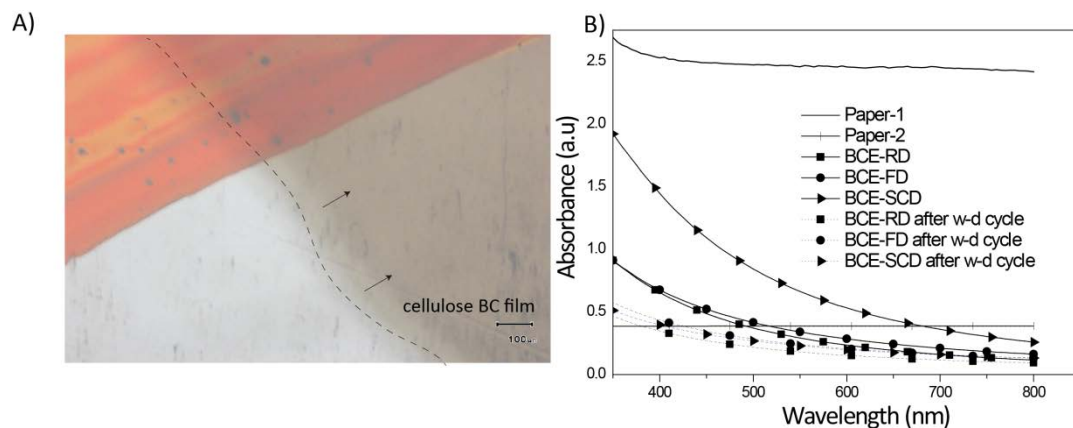
Figure 5. (A) Optical image of the BCE-SCD film immersed in a petri dish with water. The red line on the Petri dish surface is clearly distinguishable through the BC film. (B) Uv-vis spectra of BC films before and after WAC and commercial papers.

Mechanical properties

Mechanical properties are a key factor for BC films to be used as reinforcing materials, sensors or scaffolds in many applications.(Yano et al. 2005) In particular, for cell studies, the possibility of tuning the mechanical properties of the scaffold for each cell type is very attractive. Biological tissues are soft and elastic and they show a broad range of Young modulus from $1.5 \times 10^4 – 3 \times 10^4$ MPa found in bones to $10^{-4} – 10^{-3}$ MPa in softer tissues such as brain tissue. (Moore et al. 2010) Numerous researchers have revealed that cells have the ability to probe and respond to the rigidity of the substrates they are grown upon.(Pelham and Wang 1997; Rowlands et al. 2008; Engler et al. 2004; Guo et al. 2006) The cellular tensegrity model attempts to suggest that the homeostatic balance of forces governs the reciprocal relationship between cells and the physical properties of their microenvironment.(Cameron et al. 2011)

Firstly, we evaluated qualitatively the elastic behavior of the films by bending them with a tweezers. Figure 6 shows a series of images of the bending test performed. We clearly see that BCE-RD and BCE-FD films fully recovered and a flat sheet was recorded again. SCD films

17

394 did not recover fully and some creased was imaged after bending, although it did not break.

395 After wetting-drying cycles, the BC films do not break, indicating that the films keep their

396 elasticity even after a WAC cycle. Films produced by GX followed the same trend, Figure S5,

397 therefore the bacterial strain do not modify their film´s elasticity. Unlike silica aerogels that

398 are brittle and fragile materials, BC aerogels have higher degree of elasticity.(Yano et al.

399 2005)
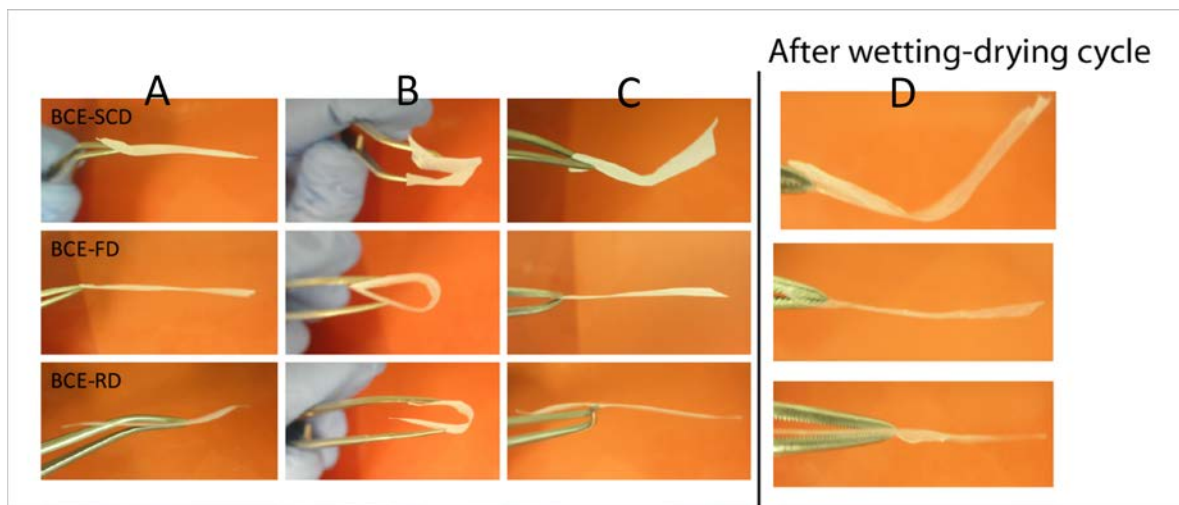
400

401 **Figure 6 Pictures of the bending test performed: (A) BCE films before the bending test**

402 **from the different drying methods, (B) process of the bending test, (C) the resulting**

403 **shapes of the BC films after the test and (D) the shape of the films obtained on a BCE**

404 **film that was wetted-dried (WAC cycle).**

405 To measure the mechanical behavior of the BC films we have used nanoindentation. For the

406 indentation cycles we used a constant maximum load of 0.4 mN to ensure that the penetration

407 depth of the tip into the films was smaller than their thickness. Smaller loads from 0.05 – 0.1

408 mN did not give us reproducible results. Moreover, we evaluated the effect of the adhesive

409 tape underneath the sample (presence and not presence) and the results did not change,

410 therefore we conclude the adhesive under the sample did not affect the measurements.

411 Figure 7 and Table 1 gather the load-displacement curves and the values obtained for the

412 penetration depth at maximum load, "*Young Modulus, E*", "*Hardness, H*" and "*elastic*

413 *parameter, EP*" for two samples (n=14). The load-displacement curves obtained are

414 representative of a material with elastoplastic properties. BC films show similar load-

415 displacement curves except for BCX-RD and BCX-FD that show lower penetration depths

416 and steeper unloading curves.

417 The analysis of the load-displacement curves shows that the BC films have creep and some

418 literature review this property as a very desirable for scaffolds that interact with

419 cells.(Cameron et al. 2011) Although we have use the slope of the curve to calculate the

420 "*Young Modulus*", ("*E*") we have to notice that this estimation is not completely correct as the

421 material has a strong elastoplastic behavior, as it happens in soft tissues. The analysis of "*E*"

422 shows that GE affords less stiff films than GX and they are independent of the drying method,

423 while BCX films are sensitive to the drying method obtaining stiffer BC films if we dry them

424 by RD or FD.

425 The "*E*" values obtained are around 200 MPa except for BCX-RD and BCX-FD that we

426 observed E of 600 MPa, suggesting that their stiffness could be comparable to tissues as bone

427 $(1.5 \times 10^4 - 3 \times 10^4$ MPa) and of soft arteries (0.1 – 1 MPa).(Moore et al. 2010)
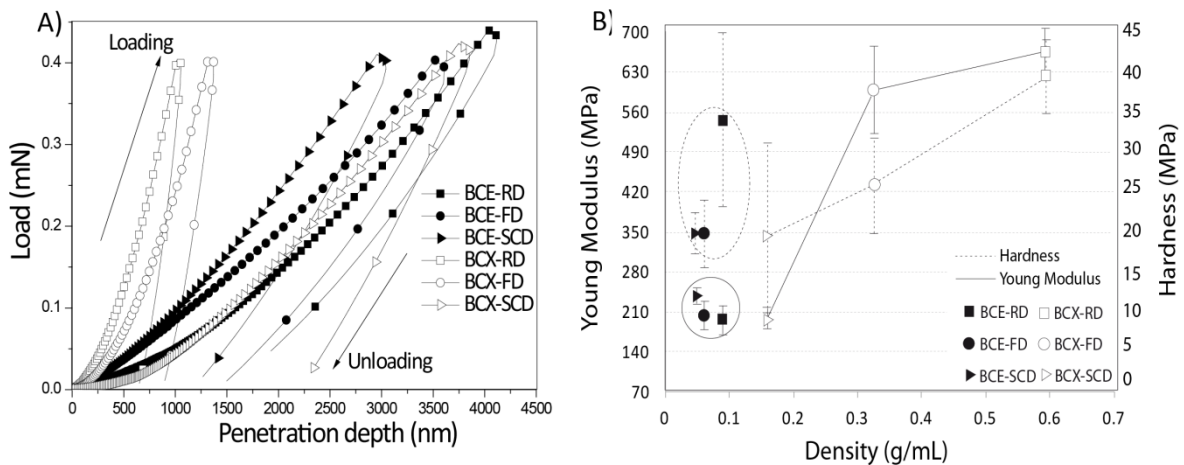
428

429 **Figure 7. (A) Representative loading-unloading curve for each BC film obtained using**

430 **the nanoindenter under a load of 0.4 mN. (B) Mean values of "*Young Modulus*", ("*E*")**

431 **and *Hardness* ("*H*") obtained for each BC film as a function of their density (n=14). We**

432 **circled the "*E*" and "*H*" for BCE for clarity.**

19

433   The averaged measured *Hardness* values ("*H*") of BC samples are around 20 – 34 MPa,

434   which indicates the resistance of BC films to the nanoindenter, BC-RD films shows higher

435   "*H*" values than the others BC films. The elastic component of the BC films was analyzed

436   using the *elastic parameter* ("*EP*").(Moner-Girona et al. 1999) BC films presenting large

437   *"Young modulus"* (BCX-RD and BCX-FD) also exhibit a low elastic character. On the other

438   side, "*E*" and penetration depth at 0.4 mN values for BCE films are similar to the values found

439   for BCX-SCD film even though they present a much smaller density (0.5- 0.8 g/cm^3 for BCE

440   and 0.16 g/cm^3 for BCX-SCD) possibly pointing to a different mechanical strength of the

441   cellulose microfibrils for each strain. The evaluation of the mechanical parameters with the

442   density shows that the combination of BCX and the drying method used allow us to obtain

443   broader range of mechanical properties for BCX films than for the BCE films.
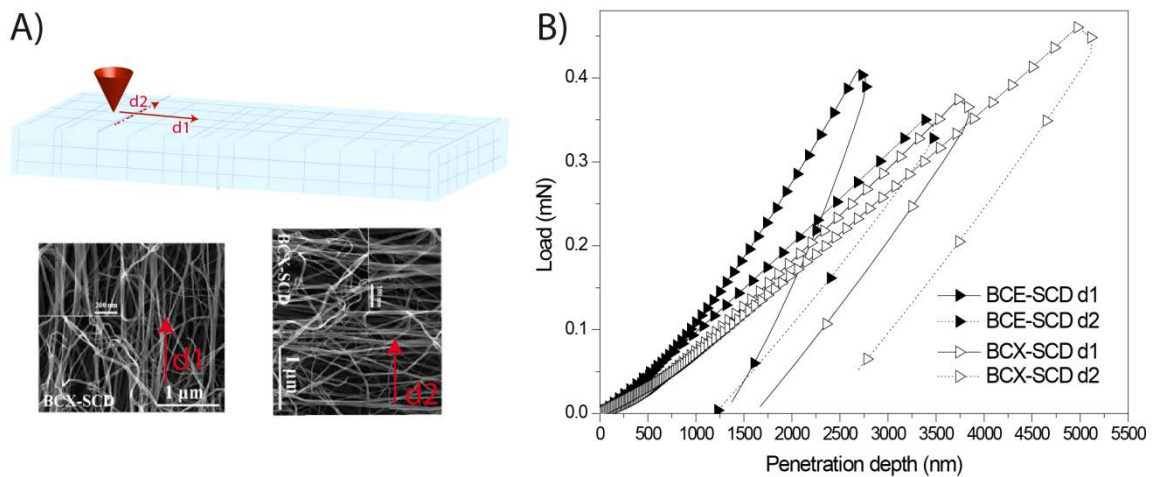
444

Figure 8. A) Schematic representation of the mechanical measurements performed over
two different directions. B) Load- displacement curves for BC films dried on SCD
conditions for the two bacterial strains.

448

	BCE-d1	BCE-d2	BCX-d1	BCX-d2
"Young modulus, E" MPa	233±50	300±50	150±40	242±100
Penetration depth at 0.4 mN (µm)	3.1±0.5	3.5±0.9	4.9±0.8	4.4±0.7

449

Table 2. Values of "*Young Modulus*" (MPa) and penetration depth at 0.4mN (µm) from

BC films dried in SCD conditions measured in two directions of the BC films.

BC- SCD films show in SEM images some anisotropy, possible directionality of the fibers therefore we evaluated "*E*" and penetration depth if we placed the sample in two opposite directions. The load-displacement curves show different profiles as a function of the direction of the measurement, Figure 8. The evaluation of "*E*" of BC-SCD show some anisotropy in the measurements although the penetration depth remains unchanged. We found for BCX-SCD and BCE-SCD a difference in "*E*" as a function of the direction where we performed the nanoindentation measurements. These results confirm the SEM images that we observed some directionality of the fibers in BCX-SCD; we also found some directionality in BCE-SCD even though we could not detect it in SEM, Table 2. We believe these are interesting results that recommend a further and deeper analysis of the mechanical properties of the BC-SCD films that will be continued with extensive loads, time and different humidity conditions, since BC-SCD films also offer high absorption capacity.

Conclusions

The use of two strains and three drying methods allowed us to obtain different BC thin films with different structural properties that can improve their application in cellulose composites materials and others. Room temperature drying, freeze-drying, and supercritical drying methods modify the porosity, mechanical properties and water absorption capability of the BC films expanding their range of the properties.

Even after 10 days of culturing, BCE films are more transparent and lighter independently of the drying methods used in comparison to BCX films, harvested for 5 days. BCE-SCD shows the highest water absorbance capacity that allow us to suggest BCE films as suitable candidates for applications such as absorbents, removal of contaminants or wound healing dressings.(Jin et al. 2011) Even though BCE films production cost would be higher, BCE-

476 SCD film could provide cellulose composites with high loading efficiencies and

477 homogeneous mixtures. Additionally the use of SCD drying improves the cristallinity of the

478 cellulose fibers.

479 BC films from GX source offer a more versatile platform since we can control the porosity,

480 mechanical properties and water absorption capacity with only one-step, selecting the

481 appropriate drying method. Additionally, GX strain offers the advantage of faster production

482 of BCX films. We hypothesize that these films could be good candidates to interface with

483 tissues since their mechanical properties could be tailored to mimic the final tissue

484 replacement and their mechanical properties are not hampered in aqueous media.

485

486 **Supporting Information**

487 Supporting Information is available online or from the author.

488

499

500

Notes and references

Institut Ciència de Materials de Barcelona, Campus UAB, 08193 Bellaterra, Spain.

E-mail: alaromaine@icmab.es

Andrade F, Alexandre N, Amorim I, Gartner F, Mauricio A, Luis AL, Gama M (2013) Studies on the biocompatibility of bacterial cellulose. J Bioact Compatible Polym 28 (1):97-112

Andrés Barrao C, Falquet L, Calderon Copete S, Descombes P, Perez R, Ortega Pérez R, Barja F (2011) Genome sequences of the high-acetic acid-resistant bacteria Gluconacetobacter europaeus LMG 18890T and G. europaeus LMG 18494 (reference strains), G. europaeus 5P3, and Gluconacetobacter oboediens 174Bp2 (isolated from vinegar). J Bacteriol 193 (10):2670-2671

Atalla RH, Vanderhart DL (1984) Native Cellulose: A Composite of Two Distinct Crystalline Forms. Science 223 (4633):283-285. doi:10.1126/science.223.4633.283

Budunoglu H, Yildirim A, Guler MO, Bayindir M (2011) Highly Transparent, Flexible, and Thermally Stable Superhydrophobic ORMOSIL Aerogel Thin Films. ACS Appl Mater & Interf 3 (2):539-545. doi:10.1021/am101116b

Cai J, Kimura S, Wada M, Kuga S, Zhang L (2008) Cellulose aerogels from aqueous alkali hydroxide-urea solution. ChemSusChem 1 (1-2):149-154

Cameron AR, Frith JE, Cooper-White JJ (2011) The influence of substrate creep on mesenchymal stem cell behaviour and phenotype. Biomaterials 32 (26):5979-5993. doi:http://dx.doi.org/10.1016/j.biomaterials.2011.04.003

Czaja WK, Young DJ, Kawecki M, Brown RM (2007) The future prospects of microbial cellulose in biomedical applications. Biomacromolecules 8 (1):1-12. doi:10.1021/bm060620d

Das K, Ray D, Bandyopadhyay NR, Sengupta S (2010) Study of the Properties of Microcrystalline Cellulose Particles from Different Renewable Resources by XRD, FTIR, Nanoindentation, TGA and SEM. J Polym Environ 18 (3):355-363

Dietrich A, Goring DAI, Revol JF (1987) Effect of mercerization on the crystallite size and crystallinity index in cellulose from different sources. Can J Chem 65 (8):1724-1725

Engler A, Bacakova L, Newman C, Hategan A, Griffin M, Discher D (2004) Substrate Compliance versus Ligand Density in Cell on Gel Responses. Biophys J 86 (1):617-628. doi:http://dx.doi.org/10.1016/S0006-3495(04)74140-5

Ennajih H, Bouhfid R, Essassi E, Bousmina M, El Kadib A (2012) Chitosan–montmorillonite bio-based aerogel hybrid microspheres. Microporous Mesoporous Mater 152:208-213

Fu L, Zhang J, Yang G (2013) Present status and applications of bacterial cellulose-based materials for skin tissue repair. Carbohydr Polym 92 (2):1432-1442. doi:http://dx.doi.org/10.1016/j.carbpol.2012.10.071

George J, Ramana KV (2005). Int J Biol Mole 37:189

George J, Sajeevkumar VA, Kumar R, Ramana KV, Sabapathy SN, Bawa AS (2008) Enhancement of thermal stability associated with the chemical treatment of bacterial (Gluconacetobacter xylinus) cellulose. J Appl Polym Sci 108 (3):1845-1851. doi:10.1002/app.27802

Guo W-h, Frey MT, Burnham NA, Wang Y-l (2006) Substrate Rigidity Regulates the Formation and Maintenance of Tissues. Biophys J 90 (6):2213-2220

Hendel T, Lesnyak V, Kuhn L, Herrmann AK, Bigall NC, Borchardt L, Kaskel S, Gaponik N, Eychmuller A (2013) Mixed Aerogels from Au and CdTe Nanoparticles. Adv Funct Mater 23 (15):1903-1911. doi:10.1002/adfm.201201674

http://www.ricoh.com/about/company/technology/tech/033.html.

549   Hu W, Chen S, Yang J, Li Z, Wang H (2014) Functionalized bacterial cellulose derivatives
550   and nanocomposites. Carbohydr Polym 101:1043-1060.
551   doi:10.1016/j.carbpol.2013.09.102
552   Jin H, Kettunen M, Laiho A, Pynnonen H, Paltakari J, Marmur A, Ikkala O, Ras RHA (2011)
553   Superhydrophobic and Superoleophobic Nanocellulose Aerogel Membranes as
554   Bioinspired Cargo Carriers on Water and Oil. Langmuir 27 (5):1930-1934.
555   doi:10.1021/la103877r
556   Kalia S, Kaith BS, Kaur I (2011) Cellulose Fibers: Bio- and Nano-Polymer Composites.
557   Springer, Berlin
558   Kim S, Kim HJ, Jeon NL (2010) Biological applications of microfluidic gradient devices.
559   Integrative Biol 2 (11-12):584-603. doi:10.1039/c0ib00055h
560   Klemm D, Heublein B, Fink. HP, Bohn A (2005) Cellulose:Fascinating Biopolymer and
561   Sustainable Raw Material. Angew Chem 44:3358-3393
562   Klemm D, Kramer F, Moritz S, Lindström T, Ankerfors M, Gray D, Dorris A (2011)
563   Nanocelluloses: A New Family of Nature-Based Materials. Angew Chem Int Ed 50
564   (24):5438-5466. doi:10.1002/anie.201001273
565   Klemm D, Schumann D, Udhardt U, Marsch S (2001) Bacterial synthesized cellulose -
566   artificial blood vessels for microsurgery. Prog Polym Sci 26:1561-1603
567   Liebner F, Haimer E, Wendland M, Neouze MA, Schlufter K, Miethe P, Heinze T, Potthast A,
568   Rosenau T (2010) Aerogels from Unaltered Bacterial Cellulose: Application of
569   scCO(2) Drying for the Preparation of Shaped, Ultra-Lightweight Cellulosic Aerogels.
570   Macromol Biosci 10 (4):349-352. doi:10.1002/mabi.200900371
571   Mansikkamaki P, Lahtinen M, Rissanen K (2007) The conversion from cellulose I to cellulose
572   II in NaOH mercerization performed in alcohol–water systems: An X-ray powder
573   diffraction study. Carbohydr Polym 68 (1):35-43. doi:10.1016/j.carbpol.2006.07.010
574   Martin L, Osso JO, Ricart S, Roig A, Garcia O, Sastre R (2008) Organo-modified silica
575   aerogels and implications for material hydrophobicity and mechanical properties. J
576   Mater Chem 18 (2):207-213. doi:10.1039/b712553d
577   Mecklenburg M, Schuchardt A, Mishra YK, Kaps S, Adelung R, Lotnyk A, Kienle L, Schulte
578   K (2012) Aerographite: Ultra Lightweight, Flexible Nanowall, Carbon Microtube
579   Material with Outstanding Mechanical Performance. Adv Mater 24 (26):3486-3490.
580   doi:10.1002/adma.201200491
581   Moner-Girona M, Roig A, Benito M, Molins E (2003) Aerogel thin film synthesis by a
582   supercritical fluid-assisted sol-gel route in a single processing unit. J Mater Chem 13
583   (9):2066-2068. doi:10.1039/b307057c
584   Moner-Girona M, Roig A, Molins E, Martinez E, Esteve J (1999) Micromechanical properties
585   of silica aerogels. Appl Phys Lett 75 (5):653-655. doi:10.1063/1.124471
586   Moore SW, Roca-Cusachs P, Sheetz MP (2010) Stretchy Proteins on Stretchy Substrates: The
587   Important Elements of Integrin-Mediated Rigidity Sensing. Dev Cell 19 (2):194-206.
588   doi:http://dx.doi.org/10.1016/j.devcel.2010.07.018
589   Murillo-Cremaes N, López-Periago AM, Saurina J, Roig A, Domingo C (2010) A clean and
590   effective supercritical carbon dioxide method for the host–guest synthesis and
591   encapsulation of photoactive molecules in nanoporous matrices. Green Chemistry 12
592   (12):2196. doi:10.1039/c004762g
593   Mwaikambo LY, Ansell MP (2001) The determination of porosity and cellulose content of
594   plant fibers by density methods. J Mater Sci Lett 20 (23):2095-2096.
595   doi:10.1023/a:1013703809964
596   Nata IF, Sureshkumar M, Lee C-K (2011) One-pot preparation of amine-rich
597   magnetite/bacterial cellulose nanocomposite and its application for arsenate removal.
598   RSC Advances 1 (4):625-631. doi:10.1039/c1ra00153a

Pelham RJ, Wang Y-l (1997) Cell locomotion and focal adhesions are regulated by substrate flexibility. Proceedings of the National Academy of Sciences 94 (25):13661-13665

Pinto RJB, Neves MrC, Neto CP, Trindade T (2012) Composites of Cellulose and Metal Nanoparticles, Nanocomposites - New Trends and Developments. Nanocomposites - New Trends and Developments. InTech, September 27, 2012 under CC BY 3.0 license. doi:10.5772/50553

Ross P, Mayer R, Benziman M (1991) Cellulose biosynthesis and function in bacteria. Microbiol Rev 55 (1):35-58

Rowlands AS, George PA, Cooper-White JJ (2008) Directing osteogenic and myogenic differentiation of MSCs: interplay of stiffness and adhesive ligand presentation. American Journal of Physiology - Cell Physiology 295 (4):C1037-C1044. doi:10.1152/ajpcell.67.2008

Russler A, Wieland M, Bacher M, Henniges U, Miethe P, Liebner F, Potthast A, Rosenau T (2012) AKD-Modification of bacterial cellulose aerogels in supercritical CO_2. Cellulose 19 (4):1337-1349

S. Hestrin MS (1954) Synthesis of Cellulose by Acetobacter xylinum. Biochem J 58:345-353

Sai H, Xing L, Xiang J, Cui L, Jiao J, Zhao C, Li Z, Li F (2013) Flexible aerogels based on an interpenetrating network of bacterial cellulose and silica by a non-supercritical drying process. Journal of Materials Chemistry A 1 (27):7963-7970. doi:10.1039/c3ta11198a

Saska S, Teixeira LN, de Oliveira PT, Gaspar AMM, Ribeiro SJL, Messaddeq Y, Marchetto R (2012) Bacterial cellulose-collagen nanocomposite for bone tissue engineering. J Mater Chem 22 (41):22102-22112. doi:10.1039/c2jm33762b

Schutz C, Sort J, Bacsik Z, Oliynyk V, Pellicer E, Fall A, Wagberg L, Berglund L, Bergstrom L, Salazar-Alvarez G (2012) Hard and Transparent Films Formed by Nanocellulose-TiO2 Nanoparticle Hybrids. Plos One 7 (10). doi:10.1371/journal.pone.0045828

Segal L, Creely JJ, Martin AE, Conrad CM (1959) An Empirical Method for Estimating the Degree of Crystallinity of Native Cellulose Using the X-Ray Diffractometer. Textile Research Journal 29 (10):786-794. doi:10.1177/004051755902901003

Sehaqui H, Zhou Q, Ikkala O, Berglund LA (2011) Strong and Tough Cellulose Nanopaper with High Specific Surface Area and Porosity. Biomacromolecules 12 (10):3638-3644. doi:10.1021/bm2008907

Shezad O, Khan S, Khan T, Park JK (2010) Physicochemical and mechanical characterization of bacterial cellulose produced with an excellent productivity in static conditions using a simple fed-batch cultivation strategy. Carbohydr Polym 82 (1):173-180. doi:http://dx.doi.org/10.1016/j.carbpol.2010.04.052

Shi ZJ, Zhang Y, Phillips GO, Yang G (2014) Utilization of bacterial cellulose in food. Food Hydrocolloids 35:539-545. doi:10.1016/j.foodhyd.2013.07.012

Siro I, Plackett D (2010) Microfibrillated cellulose and new nanocomposite materials: a review. Cellulose 17 (3):459-494. doi:10.1007/s10570-010-9405-y

Sun CC (2005) True density of microcrystalline cellulose. J Pharm Sci 94 (10):2132-2134. doi:10.1002/jps.20459

Svensson A, Nicklasson E, Harrah T, Panilaitis B, Kaplan DL, Brittberg M, Gatenholm P (2005) Bacterial cellulose as a potential scaffold for tissue engineering of cartilage. Biomaterials 26 (4):419-431. doi:http://dx.doi.org/10.1016/j.biomaterials.2004.02.049

Ul-Islam M, Khan T, Park JK (2012a) Nanoreinforced bacterial cellulose–montmorillonite composites for biomedical applications. Carbohydr Polym 89 (4):1189-1197. doi:http://dx.doi.org/10.1016/j.carbpol.2012.03.093

Ul-Islam M, Khan T, Park JK (2012b) Water holding and release properties of bacterial cellulose obtained by in situ and ex situ modification. Carbohydr Polym 88 (2):596-603. doi:10.1016/j.carbpol.2012.01.006

650 Ul-Islam M, Shah N, Ha JH, Park JK (2011) Effect of chitosan penetration on physico-
651   chemical and mechanical properties of bacterial cellulose. Korean J Chem Eng 28
652   (8):1736-1743. doi:10.1007/s11814-011-0042-4
653 Ummartyotin S, Juntaro J, Sain M, Manuspiya H (2012) Development of transparent bacterial
654   cellulose nanocomposite film as substrate for flexible organic light emitting diode
655   (OLED) display. Ind Crop Prod 35 (1):92-97. doi:10.1016/j.indcrop.2011.06.025
656 Wang Y, Zhao Y, Deng Y (2008) Effect of enzymatic treatment on cotton fiber dissolution in
657   NaOH/urea solution at cold temperature. Carbohydr Polym 72 (1):178-184
658 Wicklein B, Salazar-Alvarez G (2013) Functional hybrids based on biogenic nanofibrils and
659   inorganic nanomaterials. Journal of Materials Chemistry A 1 (18):5469-5478.
660   doi:10.1039/c3ta01690k
661 Wu Z-Y, Li C, Liang H-W, Chen J-F, Yu S-H (2013) Ultralight, Flexible, and Fire-Resistant
662   Carbon Nanofiber Aerogels from Bacterial Cellulose. Angew Chem Int Ed 52
663   (10):2925-2929. doi:10.1002/anie.201209676
664 Yamada Y, Hoshino K, Ishikawa T (1997) The phylogeny of acetic acid bacteria based on the
665   partial sequences of 16S ribosomal RNA: the elevation of the subgenus
666   Gluconoacetobacter to the generic level. Biosci, Biotechnol, Biochem 61 (8):1244-
667   1251
668 Yano H, Sugiyama J, Nakagaito AN, Nogi M, Matsuura T, Hikita M, Handa K (2005)
669   Optically transparent composites reinforced with networks of bacterial nanofibers.
670   Adv Mater 17 (2):153-+. doi:10.1002/adma.200400597
671 Zhang L, Ruan D, Zhou J (2001) Structure and Properties of Regenerated Cellulose Films
672   Prepared from Cotton Linters in NaOH/Urea Aqueous Solution. Industrial &
673   Engineering Chemistry Research 40 (25):5923-5928
674
675

Figures and Tables

Figure 1. A) Picture of a BC layer on top of the bacteria culture liquid media. B) Cleaned BC films obtained after the NaOH treatment. C) Picture show a final BC film dried and the accordion setup were BC films are held during the drying process.

Figure 2. A) X-ray diffraction pattern for 1) BCE- room temperature, 2) freeze drying 3) supercritical drying and 4) non cleaned BCE film. B) FTIR spectra for a non-cleaned BCE film and a BCE film after cleaning.

Figure 3. SEM images of the BC films obtained after different drying conditions. Inserts show higher magnification images of the films.

Figure 4. A) Percentage of the water absorbed in the BC films after three wetting-drying cycles. B) Images of the BCE-SCD films and lens paper before and after wetting.

Figure 5. A) Optical image of the BCE-SCD film immersed in a petri dish with water. The red line on the Petri dish surface is clearly distinguishable. B) Uv-vis spectra of the papers before and after WAC in comparison to commercial papers.

Figure 6. Pictures of the bending test performed: A) BCE films before the bending test from the different drying methods, B) process of the bending test, C) the resulting shapes of the BC films after the test and D) the shape of the films obtained on a BCE film that was wetted-dried (WAC cycle).

Figure 7. A) Representative loading-unloading curve for each BC film obtained using the nanoindenter under a load of 0.4 mN. B) Mean values of Young Modulus (E) and

702   **Hardness (H) obtained for each BC film as a function of their density. (14 measurements**

703   **for each sample).**

704

705   **Figure 8. A) Schematic representation of the mechanical measurements performed over**

706   **two different directions. B) Load- displacement curves for BC films dried on SCD**

707   **conditions for the two bacterial strains.**

708

709   **Table 1. Summary of the structural and mechanical values obtained for the BC films.**

710

711   **Table 2 Values of "*Young Modulus*" (MPa) and penetration depth at 0.4mN (µm) from**

712   **BC films dried in SCD conditions measured in two directions of the BC films.**

713

714

715 **Figure 1. A) Picture of a BC layer on top of the bacteria culture liquid media. B)**

716 **Cleaned BC films obtained after the NaOH treatment. C) Picture show a final BC film**

717 **dried and the accordion setup were BC films are held during the drying process.**
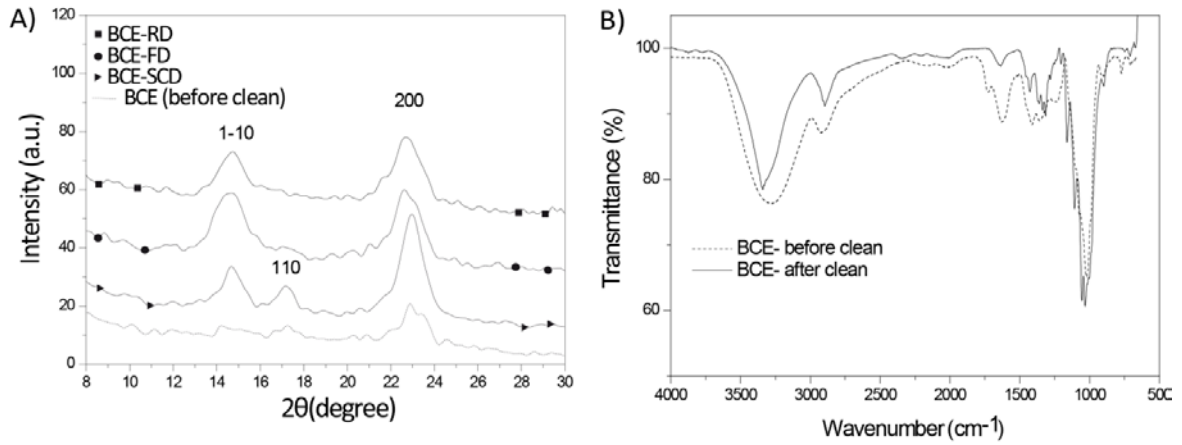
718
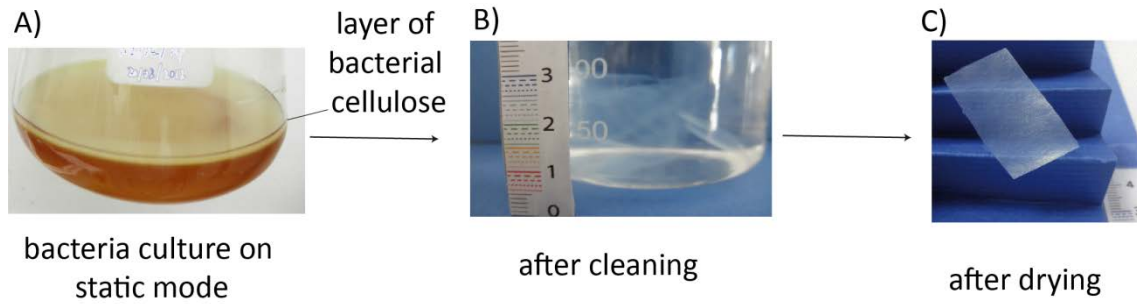
719

720

721

722   **Figure 2. A) X-ray diffraction pattern for 1) BCE- room temperature, 2) freeze drying 3)**

723   **supercritical drying and 4) non cleaned BCE film. B) FTIR spectra for a non-cleaned**

724   **BCE film and a BCE film after cleaning.**

725

726

727 **Figure 3. SEM images of the BC films obtained after different drying conditions. Inserts**

728 **show higher magnification images of the films.**
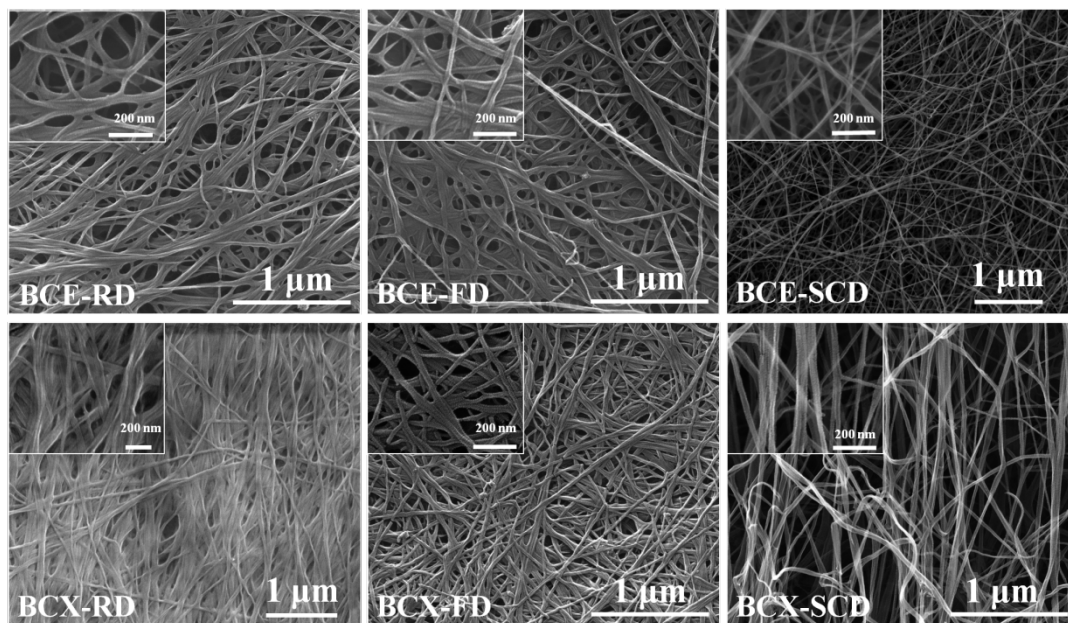
729
730

731   **Figure 4. A) Percentage of the water absorbed in the BC films after three wetting-drying**

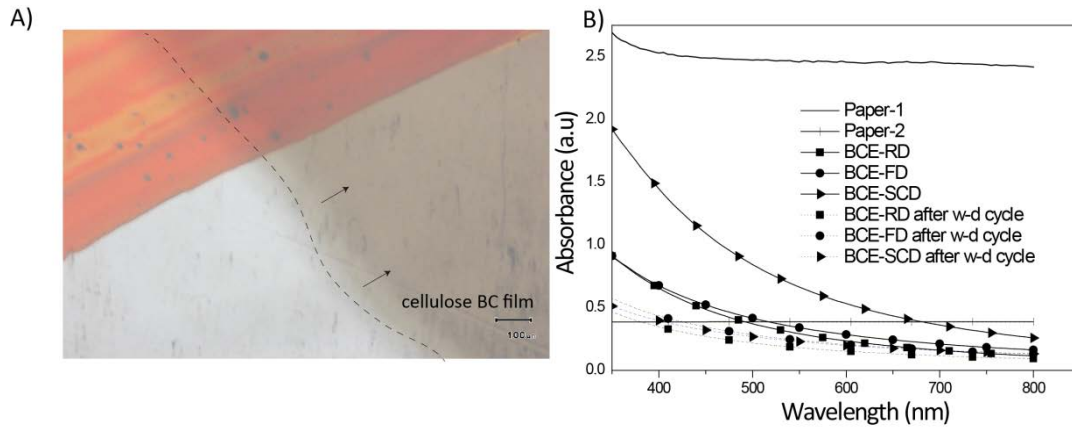732   **cycles. B) Images of the BCE-SCD films and lens paper before and after wetting.**
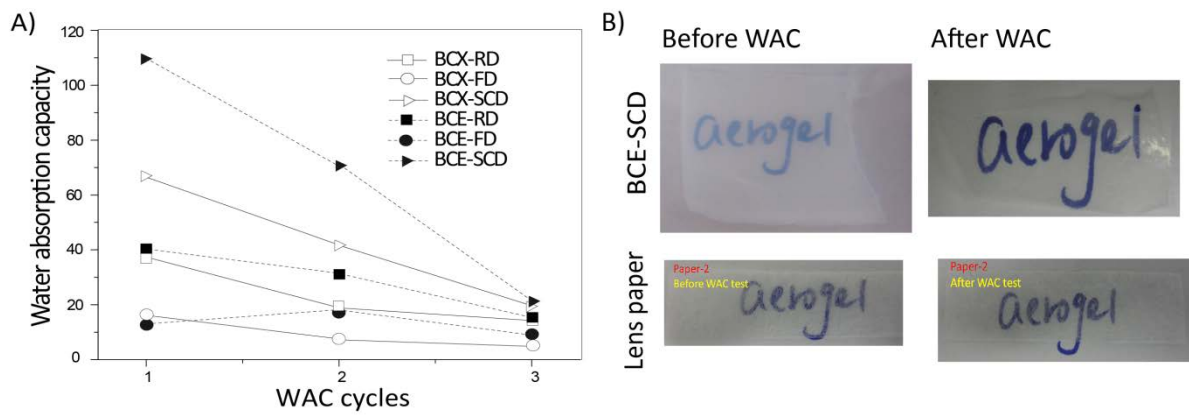

733

734

735   **Figure 5. A) Optical image of the BCE-SCD film immersed in a petri dish with water.**

736   **The red line on the Petri dish surface is clearly distinguishable. B) Uv-vis spectra of the**

737   **papers before and after WAC in comparison to commercial papers.**

738

739

Figure 6 shows pictures of the bending test performed: A) BCE films before the bending test from the different drying methods, B) process of the bending test, C) the resulting shapes of the BC films after the test and D) the shape of the films obtained on a BCE film that was wetted-dried (WAC cycle).
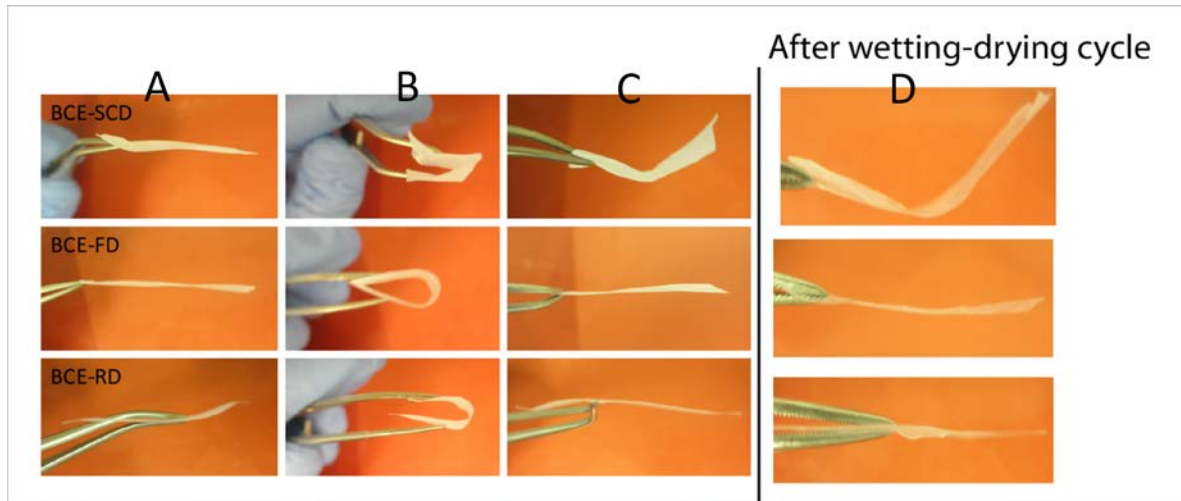
Figure 7. A) Representative loading-unloading curve for each BC film obtained using the nanoindenter under a load of 0.4 mN. B) Mean values of "*Young Modulus*", ("*H*") and *Hardness* ("*H*") obtained for each BC film as a function of their density (n=14). We circled the"*E*"and "*H*" for BCE for clarity.
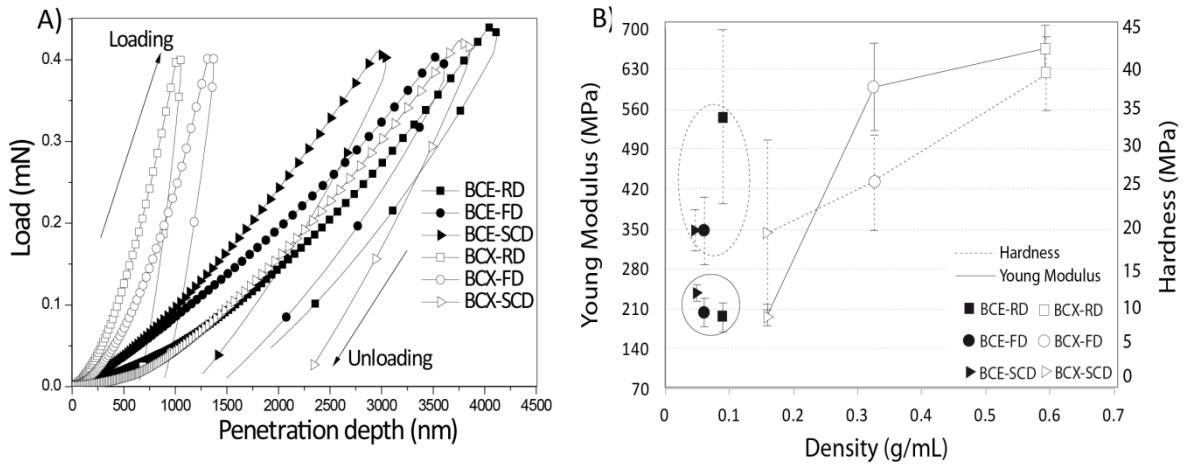
752 **Figure 8. A) Schematic representation of the mechanical measurements performed over**

753 **two different directions. B) Load- displacement curves for BC films dried on SCD**

754 **conditions for the two bacterial strains.**
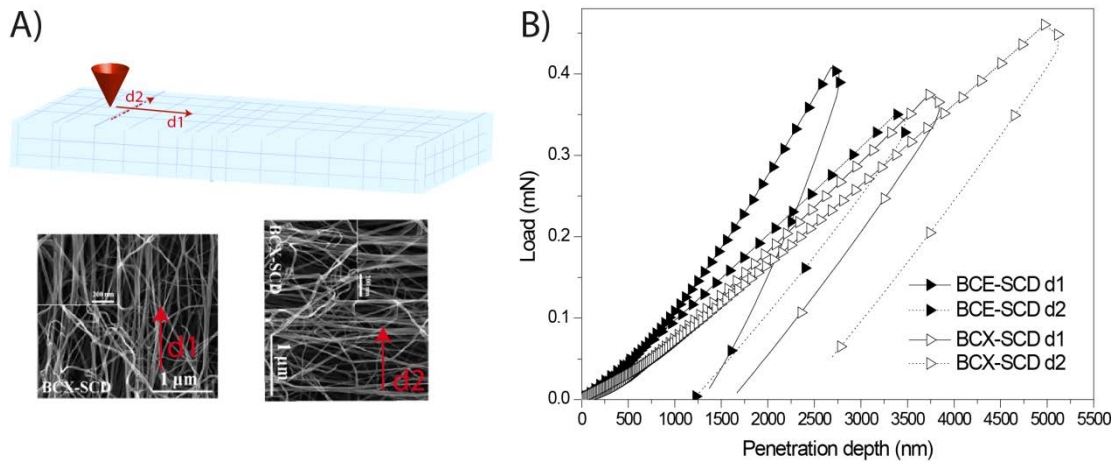
755

756

757

758

759

760

Table 1. Summary of the structural and mechanical values obtained for the BC films.

762

	Drying method	RD		FD		SCD	
	Strain	**BCE**	**BCX**	**BCE**	**BCX**	**BCE**	**BCX**
Structural	Film Thickness (μm)	24±2	37±2	34±2	40±4	58±3	67±2
	Density (g/mL)	0.08± 0.01	0.59± 0.03	0.06± 0.01	0.32± 0.02	0.05± 0.01	0.16± 0.01
	Total Porosity (%)	94±2	60±2	95 ±2	79±2	96±2	89±2
	Fibers diameter (nm)	17±2	19±3	20±4	19±3	16±2	20±4
	WAC 1st cycle	39.5	37.3	15.8	15. 8	109.4	66.6
	WAC after 3 cycles	15.3	14.2	92.3	50.2	19.8	19.4
	WAC Decrease (%)	61	62	42	68	82	71
Mechanical	Penetration depth at 0.4mN load (μm)	3.9±0.4	1.1±0.1	4.1±0.4	1.4±0.3	3.2±0.5	4.3± 1.5
	Young modulus ("E")(MPa)	198±46	659±85	204±46	601±155	238±25	198±34
	Hardness ("H")(MPa)	34±22	39±9	20±8	26±12	20±5	19±21
	EP (%)	59±7	39±3	53±4	33±3	52±5	48±13

763

764

765 **Table 2 Values of "*Young Modulus*" (MPa) and penetration depth at 0.4mN (µm) from**

766 **BC films dried in SCD conditions measured in two directions of the BC films.**

	BCE-d1	BCE-d2	BCX-d1	BCX-d2
"Young modulus, E" MPa	233±50	300±50	150±40	242±100
Penetration depth at 0.4 mN (µm)	3.1±0.5	3.5±0.9	4.9±0.8	4.4±0.7

767

768

769

Supplementary Material

Click here to download Supplementary Material: Supporting Information Cellulose.pdf